HOKA: A New Isolated Current Measuring Principle and its Features

Nicolas Karrer
Swiss Federal Institute of Technology
Electrical Engineering and Design Lab (EEK)
Gloriastrasse 35 / ETZ
CH-8092 Zürich
Switzerland
karrer@eek.ee.ethz.ch

Patrick Hofer-Noser
Atlantis Solar Systems
Lindenrain 4
CH-3012 Bern
Switzerland
hofer@atlantisenergy.ch

Daniel Henrard
LEM SA
Case Postale 785
CH-1212 Grand-Lancy 1
Switzerland
dhe@lem.com

Abstract– **The new current measuring principle HOKA is presented. Probes based on this principle can measure DC currents of several hundred amps, as well as di/dt's of several kA/μs. A measurement setup to generate these di/dt's as well as a current probe based on the HOKA principle were built. With the setup the current probe was tested and compared with other state of the art current probes.**

I. Introduction

To measure currents of power electronic systems in the range of hundred to some thousand amps probes based on the induction law are often employed. The most known are the Rogowski coil [1], [2], [3], [4], [5], and the current transformer [6], [7], [8]. Shunts are not often employed because of their galvanic coupling and power losses. The main problem when using one of the former two current measuring devices is the inability to measure DC currents. When paralleling IGBT's [9] high di/dt's as well as DC currents must be measured. DC currents can be measured with Hall sensors or with magnetoresisive sensors. The idea of merging the output signal of a slow and a fast device in a control loop is not new [10]. In the following a new method is presented which measures currents without a feedback control.

II. The New Principle

An overview of the current probe based on the new measuring principle is depicted in Fig. 1. The probe consists of an evaluation circuit and two different types of current sensors: one or several Hall sensors and an air or Rogowski coil. To illustrate how this new principle works, the transfer function

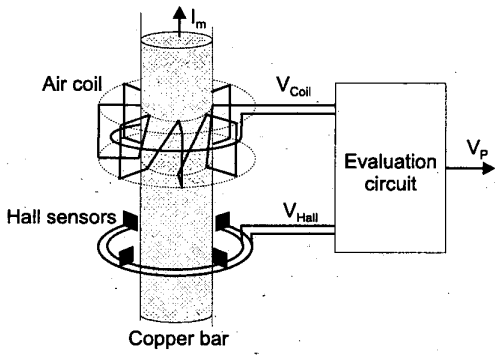

Fig. 1. Current probe overview

(TF) of the sensors must be examined. One sensor type must have an output signal which is proportional to the sensed signal. Hall sensors exhibit this property when measuring electrical current. Its TF can be approximated by a low-pass (1) where $s = j\omega$, I_m represents the monitored current, V_H the sensor's output voltage, K_H the sensitivity of the Hall sensor and T_H its time constant or $1/T_H$ its corner frequency.

$$H_{Hall}(s) = \frac{V_H}{I_m} = \frac{K_H}{s\,T_H + 1} \tag{1}$$

The other sensor type must provide an output signal which is proportional to the derivative of the sensed current. This can be achieved by an air or Rogowski coil. The TF of these coils can be approximated by (2), where V_C represents the output voltage of the coil and M the mutual inductance.

$$H_{Coil}(s) = \frac{V_C}{I_m} = s\,M \tag{2}$$

The HOKA principle is used to combine the output signals V_H and V_C in the evaluation circuit. The principle states that it is possible to combine these two signals in a way, that an unlimited bandwith is obtained. The block diagram Fig. 2 shows how the two signals are merged. Assuming that we are able to build an ideal low-pass, amplifier and adder, the TF of the probe reduces to a constant value (3).

$$H_{Probe}(s) = \frac{V_P}{I_m} = (s\,M)\left[\frac{1}{s\,T_H + 1}\,\frac{T_H\,K_s}{M}\right] + \\ + \left(\frac{K_H}{s\,T_H + 1}\right)\left[\frac{K_s}{K_H}\right] = K_s\left[\frac{s\,T_H + 1}{s\,T_H + 1}\right] = K_s \tag{3}$$

K_s is the probe's sensitivity. The main features when making use of this new principle are:

- elimination of the required integrator when employing Rogowski coils for current measurement
- ability to measure DC currents as well as high di/dt's
- delay time below 1 ns for a ramp
- no phase shift till about 50 MHz
- low insertion impedance
- electrical isolation from the monitored current
- no saturation effects
- no damage by surge currents.

0-7803-5589-X/99/$10.00 © 1999 IEEE

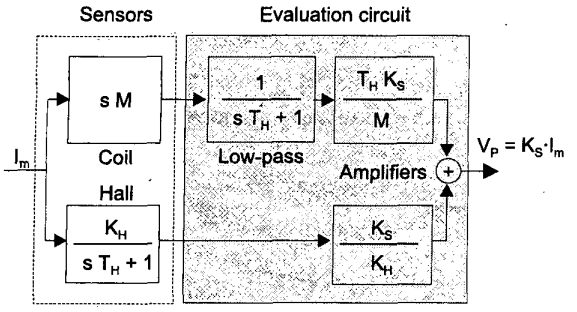

Fig. 2. Ideal HOKA principle

This principle is not restricted to current measurement but may always be used to enlarge the bandwidth of a measuring device when the monitored signal can be measured with a sensor having a proportional or low-pass TF and a second sensor having a high-pass or derivative TF.

In the following we focus on current measurement and we will analyze in detail a practical implementation of the ideal HOKA principle.

III. Practical Implementation

To implement the HOKA principle a slightly modified topology was chosen, Fig. 3, where the parameter matching is not so critical. Starting with the block diagram in Fig. 2 the two time constants T_H in the coil path of the evaluation circuit are replaced by a new time constant T_V. A low-pass is inserted at the output of the Hall sensor signal with the same time constant T_V. As long as $T_V \geq 100\,T_H$ the behavior of the evaluation circuit is only slightly altered compared with the ideal one. Having the same low-pass block in the coil and Hall signal path, it can be shifted as well as part of the amplification block past the addition block as shown in Fig. 3. As a result the matching of the parameters of the low-pass becomes easy as long as the given inequality is respected. The TF of the coil has been replaced by a more realistic model showing a resonance behavior at $f_n = 1/(2\,\pi\,T_2)$ when $T_0 \approx 1$. The ideal TF of the probe (3) is still valid till about $f_n/10$. For higher frequencies, the resonance of the coil becomes dominant an the TF of the probe can be approximated by (4).

$$H_{Probe_{HF}}(s) = \frac{V_P}{I_m} = \frac{K_s}{s^2\,T_2^2 + s\,T_1 + T_0} \tag{4}$$

A. Evaluation circuit

The block diagram of the evaluation circuit Fig. 3 has been realized as displayed in Fig. 4 [11]. The op amp A1 is a high precision amplifier while the A2 is a wideband amplifier. The TF of this circuit, with ideal amplifiers ($A_1(s) = A_2(s) = \infty$), is for the Hall path

$$H_{LP}(s) = \frac{V_0}{V_{Hall}} = -\frac{R_2}{R_{1H}}\left(\frac{1}{s\,C_2\,R_2 + 1}\right) \tag{5}$$

and for the coil path

$$H_{LP}(s) = \frac{V_0}{V_{Coil}} = -\frac{R_2}{R_{1C}}\left(\frac{1}{s\,C_2\,R_2 + 1}\right). \tag{6}$$

Even when modeling the two op amps's TF as second order low-passes, the TF remains a first order low-pass up to several MHz. To be able to reach these theoretical values, high speed design techniques must be used [12]. In order to reduce the distance between the components of the high speed path as much as possible, the layout topology has to be planned carefully.

The resistors R_{1H} and R_{1C} are used to set the correct amplification value in each path. To increase the noise immunity of the output signal, a 50 Ω termination should be used (R_{50}). The drawback of the termination is an increase of a factor two of the required amplification.

The measured Bode plot of the realized circuit is shown in Fig. 5. The solid line represents the measured data while the crosses show the theoretical plot of a first order low-pass. The circuit behaves as a low-pass for over six decades, spanning a range of 100 dB magnitude.

B. Hall sensor

The output signal of a Hall sensor is proportional to the magnetic flux density B. More precisely, it is proportional to the component of the vector $\mathbf{B}$ which is normal to the chip's surface. The Hall sensors will pick up the flux density from the

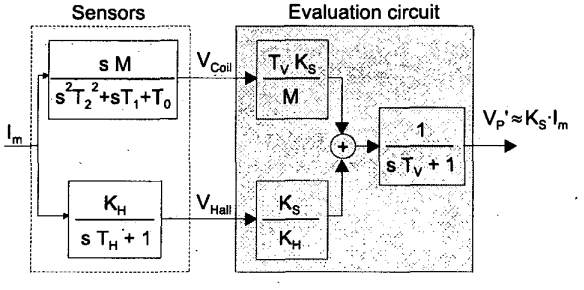

Fig. 3. Implementation of the HOKA principle

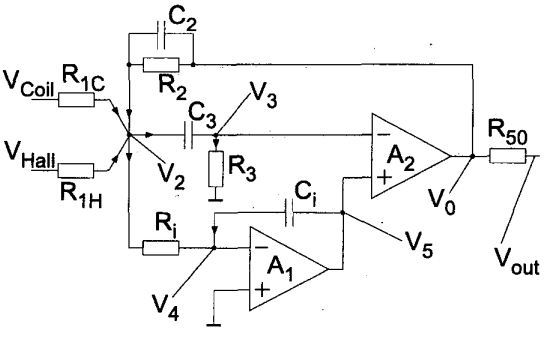

Fig. 4. Evaluation circuit

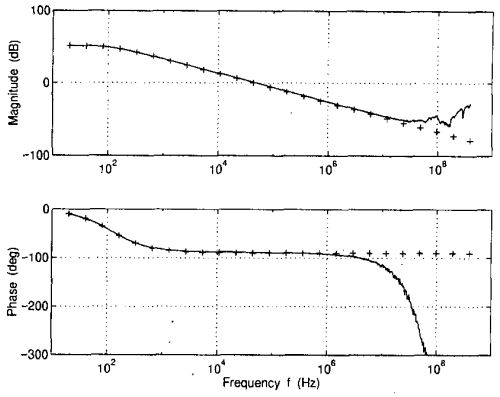

Fig. 5. Bode plot of low-pass circuit

monitored current I_m as well as the one of the return wire I_r and other stray fluxes. Since no core is used to increase the flux density generated by the monitored current, a single Hall sensor is prone to stray fields existing at the same location. This is especially true in the domain of power electronic systems.

In the following we analyzed the noise immunity of a circular Hall sensor arrangement like shown in Fig. 1 and more in detail in Fig. 6. N Hall sensors are placed on a circle of radius r_s. The sensors are equidistantly positioned with respect to each other, therefore, the angle between them is

$$\alpha_j = \frac{2\pi}{N} j. \tag{7}$$

The angle α_j represents the angle between the vector $\mathbf{r_{sj}}$ and the $\mathbf{e_x}$ axis. We assume that through the center of the circle or sligtly offset passes the wire I_m of which the current is monitored. On the outside of this circle the return wire I_r passes by. A section of this arrangement is displayed in Fig. 6. The Hall sensor is found at the end of the vector $\mathbf{r_{sj}}$ and it measures the field which is parallel to its surface normal vector $\mathbf{e_n}$. The distance from the origin to the current wire is r_r and β is the angle between $\mathbf{r_r}$ and $\mathbf{e_x}$. R_0 and r_0 are the radii of two circels. Their importance will be explained further on. Note that all the vectors named $\mathbf{e}$ are unit vectors. The index r stands for the *return* wire, m for the *monitored* wire and s for *sensor*. Assuming that the current wire or bar is a wire filament of infinite length, it is possible to compute the magnetic field and its direction in each point with the law of Biot-Savart. This filament wire extends along the $\mathbf{e_z}$ axis. Thus from the following equations (8)-(12) the magnetic field strength measured by the Hall sensor (13) can be computed.

$$\mathbf{r_{sj}} = r_s \begin{pmatrix} \cos\alpha_j \\ \sin\alpha_j \\ 0 \end{pmatrix} \tag{8}$$

$$\mathbf{e_n} = \begin{pmatrix} -\sin\alpha_j \\ \cos\alpha_j \\ 0 \end{pmatrix} \tag{9}$$

$$\mathbf{r_r} = r_r \begin{pmatrix} \cos\beta \\ \sin\beta \\ 0 \end{pmatrix} \tag{10}$$

$$\mathbf{r_{dj}} = \mathbf{r_{sj}} - \mathbf{r_r} \tag{11}$$

With the current I_r flowing along the $-\mathbf{e_z}$ axis

$$\mathbf{H_{rj}} = \frac{\mathbf{r_{dj}} \times \mathbf{e_z}}{r_{dj}} \frac{I_r}{2\pi r_{dj}} \tag{12}$$

therefore the field measured by the Hall sensor j and generated by the current I_r is

$$H_{Sj} = \mathbf{H_{rj}} \cdot \mathbf{e_n} = \\ = \frac{a\cos(\alpha_j - \beta) - 1}{1 + a^2 - 2a\cos(\alpha_j - \beta)} \frac{I_r}{2\pi r_s}. \tag{13}$$

In the last equation the factor $a = r_r / r_s$ has been introduced to simplify the equation. Three special domains of a can be identified:

- $a = 0$ then $H_{Sj} = -I_r / (2\pi r_s)$. This is the well-known case when the wire is in the center. This result can also be obtained by employing the line integral of the magnetic field strength. Each Hall sensor detects the same magnetic field strength.
- $0 < a < 1$ the wire is closer to the origin than the Hall sensor.
- $a > 1$ the Hall sensor is closer to the origin than the wire.

With (13) it is now possible to compute the measurement error if the monitored current wire I_m is not in the center and to quantify the influence on the output voltage of the return wire I_r. When N identical Hall sensors are connected in series, each Hall sensor will deliver a signal proportional to the magnetic field present at its position, $V_{Hj} = K_H H_{Sj}$. Therefore the sum of all the Hall sensor output voltages for a centered wire I_m (ideal case, $a = 0$) is:

$${}_0V_{Halls} = +K_H \sum_{j=0}^{N-1} \frac{I_m}{2\pi r_s} = +N K_H \frac{I_m}{2\pi r_s}. \tag{14}$$

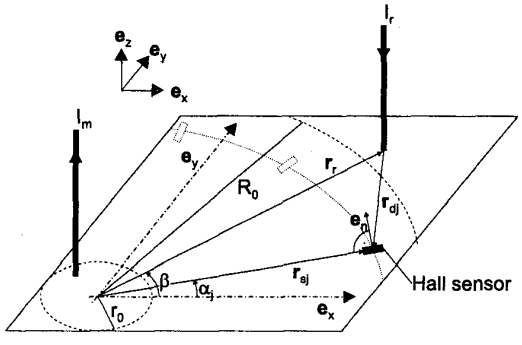

Fig. 6. Hall sensors configuration

If the wire I_m is slightly off the center (normal case, $0 < a < 1$), the following output voltage is found:

$$<V_{Halls} = -K_H \frac{I_m}{2\pi r_s} \sum_{j=0}^{N-1} \frac{a\cos(\alpha_j - \beta) - 1}{1 + a^2 - 2a\cos(\alpha_j - \beta)}. \quad (15)$$

Last we consider the output voltage caused by a wire which passes outside the circumference of the Hall sensor circle ($a > 1$). This is in most cases the return wire I_r.

$$>V_{Halls} = K_H \frac{I_r}{2\pi r_s} \sum_{j=0}^{N-1} \frac{a\cos(\alpha_j - \beta) - 1}{1 + a^2 - 2a\cos(\alpha_j - \beta)} \quad (16)$$

Note that the sign of the equations for V_{Halls} is related to the current flow direction. The relative error for an off-center wire is given in (17).

$$<err_{rel} = \frac{{}_0V_{Halls} - {}_<V_{Halls}}{{}_0V_{Halls}} = = 1 + \frac{1}{N} \sum_{j=0}^{N-1} \frac{a\cos(\alpha_j - \beta) - 1}{1 + a^2 - 2a\cos(\alpha_j - \beta)} \quad (17)$$

The relative error generated by the return wire, assuming that both wires carry the same current, is expressed in (18).

$$>err_{rel} = \frac{{}_0V_{Halls} - ({}_0V_{Halls} +_> V_{Halls})}{{}_0V_{Halls}} = = \frac{1}{N} \sum_{j=0}^{N-1} \frac{a\cos(\alpha_j - \beta) - 1}{1 + a^2 - 2a\cos(\alpha_j - \beta)} \quad (18)$$

In both cases when plotting the err_{rel} as a function of β, the maximum relative error is reached when $\beta = 0$ or $\beta = \pi/(2N)$. The interest is focused on a relative error of less than 5% so only realistic values for N have been plotted. Since the function is periodic, only a little more than one period is shown in the top drawing of Fig. 7 and Fig. 8. The different curves represent different numbers of Hall sensors, N. The lowest N is plotted as dotted line and the highest value as dashed line. The bottom drawing of Fig. 7 and Fig. 8 show the relative error (17) and (18) as a fuction of the factor a ($a = r_r/r_s$). A first interpretation is intuitive: the nearer to the center the monitored current wire is placed, the smaller is the error. The further away the return wire is from the Hall sensors, the smaller its influence. Additionally it can be seen that with a few sensors evenly distributed on the circumference but without a core, relative errors of some % can still be achieved. In our prototype a is less than 0.5 for the inner wire and more than 2.5 for the return wire. In order to not exceed a certain error, a specific a for the inner and outer wire must be preserved. This can be achieved by a case. In Fig. 6 two dashed circles are visible representing a fictive case of the probe. R_0 is the outer radius, r_0 the radius of the hole. By selecting these radii so that $a < r_0/r_s$ for the inner hole and $a > R_0/r_s$ for the boundary of the case, a specific relative error will not be exceeded.

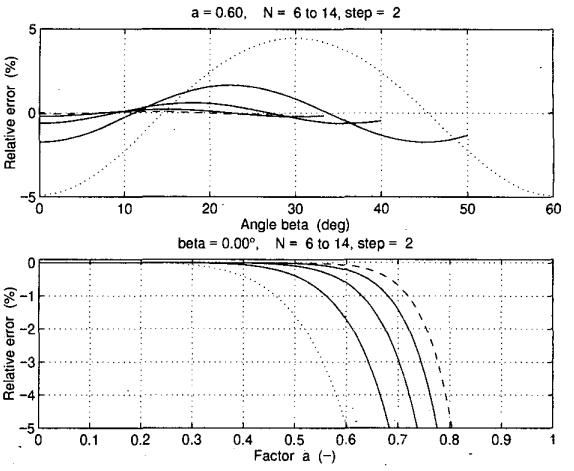

Fig. 7. Hall sensor: relative error of an off-center wire

C. Coil

The coils we have designed have their natural resonance frequency between 10 MHz and 200 MHz. They have from 10 to 100 windings, and are constructed on a multi-layer PCB [13]. The windings have a rectangular shape: from a via a track starts on the upper surface to a next via. From the bottom of this via a second track starts on the bottom surface and returns next to the first via. Here again a via for the next winding is placed. In Fig. 1 the skeleton of such a coil is depicted.

The considerations made for Hall sensors about noise immunity are also applicable to coil windings. The influence of an off-center wire I_m or the return wire I_r on the induced voltage or on the mutual inductance M is analyzed in the following. A coil, as shown in Fig. 1, consists of several windings. Each winding is connected serially to the next one. Therefore the induced voltages, the electromotive forces (emf's), will add up. Since the flux is comming from the monitored wire, the total

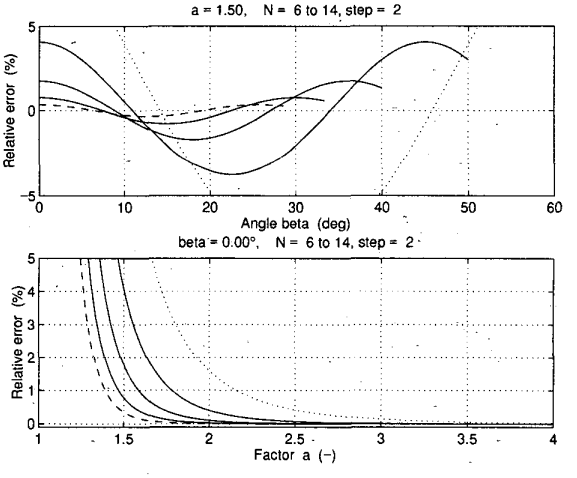

Fig. 8. Hall sensor: relative error of the return wire

emf can be written as:

$$v_{emf} = M_0 \frac{\mathrm{d}i_m}{\mathrm{d}t} + \cdots + M_{N-1} \frac{\mathrm{d}i_m}{\mathrm{d}t} = \\ = \sum_{j=0}^{N-1} M_j \frac{\mathrm{d}i_m}{\mathrm{d}t} = M \frac{\mathrm{d}i_m}{\mathrm{d}t}. \quad (19)$$

In Fig. 9 two windings of a coil and the different vectors needed for computation are shown. The vector $\mathbf{r_{wj}(q)}$ is position dependent. The variable q represents the position along the winding and ranges from $q = 0$ to $q = L$.

$$\mathbf{r_{wj}(q)} = (r_i + q) \begin{pmatrix} \cos\alpha_j \\ \sin\alpha_j \\ 0 \end{pmatrix} \quad (20)$$

with the current I_r flowing along the $-\mathbf{e_z}$ axis:

$$\mathbf{H_{rj}(q)} = \frac{\mathbf{r_{dj}(q)} \times \mathbf{e_z}}{r_{dj}(q)} \frac{I_r}{2\pi r_{dj}(q)} \quad (21)$$

$$H_{wj}(q) = \mathbf{H_{rj}(q)} \cdot \mathbf{e_n} \quad (22)$$

the flux flowing through the winding j is

$$\phi_j = b\,\mu_0 \int_0^L H_{wj}(q)\,\mathrm{d}q = \mathrm{M_j\,I_r} \quad (23)$$

therefore the mutual inductance becomes:

$$M_j = -\frac{b\,\mu_0}{4\pi} \log(\lambda_j) \quad (24)$$

$$\lambda_j = \frac{(L + r_i)^2 + (A\,r_i)^2 - 2\,A\,r_i \cos(\alpha_j - \beta)(r_i + L)}{r_i^2[1 + A^2 - 2\,A\cos(\alpha_j - \beta)]}.$$

Similar to the Hall sensor case, the following substitution has been made $A = r_r/r_i$. Distinguished values for A are:

- $A = 0$ when the wire is in the center
- $0 < A < 1$ when the wire is placed at some distance from the origin in the inner hole of the coil
- $A > (r_i + L)/r_i$ when the return wire I_r is outside the coil's windings.

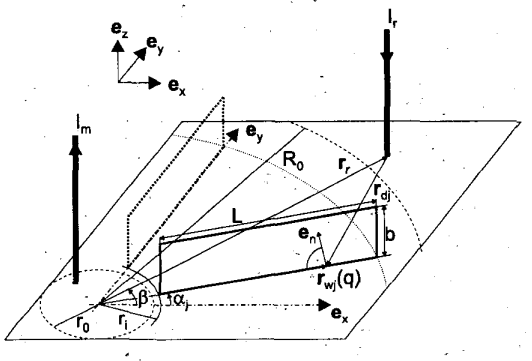

Fig. 9. Windings configuration

Note that M_j (24) is negative for $A = 0$ since the magnetic field strength generated by the return wire I_r is opposite to the normal vector $\mathbf{e_n}$ of the winding surface. The sign changes when the current is flowing along the $\mathbf{e_z}$ axis, like I_m does. Therefore, when considering the case of I_m placed in the center of the coil (ideal case, $a = 0$), the sign of (24) changes and the equation reduces to (25).

$${}_0M_j = +\frac{b\,\mu_0}{2\pi} \log\left(\frac{L + r_i}{r_i}\right) \quad (25)$$

When a coil consists of N separate windings, the mutual inductance for the centered wire I_m takes the known form of:

$${}_0M = \frac{b\,\mu_0}{4\pi} \sum_{j=0}^{N-1} \log\lambda_j = \frac{N\,b\,\mu_0}{2\pi} \log\left(\frac{L + r_i}{r_i}\right). \quad (26)$$

For the other two cases, with I_m off-center and I_r outside the coil's circumference, the mutual inductance is:

$${}_<M = \frac{b\,\mu_0}{4\pi} \sum_{j=0}^{N-1} \log\lambda_j \quad (27)$$

$${}_>M = -\frac{b\,\mu_0}{4\pi} \sum_{j=0}^{N-1} \log\lambda_j. \quad (28)$$

Employing the same relative error formulas as before, the influence of the wire position to the ideal mutual induction can be formulated as follows:

$${}_<err_{rel} = \frac{{}_0v_{emf} - {}_<v_{emf}}{{}_0v_{emf}} = 1 - \frac{{}_<M}{{}_0M} = \\ = 1 - \frac{1}{2N} \frac{1}{\log\left(\frac{L+r_i}{r_i}\right)} \sum_{j=0}^{N-1} \log\lambda_j \quad (29)$$

and for the other case

$${}_>err_{rel} = \frac{{}_0v_{emf} - ({}_0v_{emf} + {}_>v_{emf})}{{}_0v_{emf}} = -\frac{{}_>M}{{}_0M} = \\ = +\frac{1}{2N} \frac{1}{\log\left(\frac{L+r_i}{r_i}\right)} \sum_{j=0}^{N-1} \log\lambda_j. \quad (30)$$

For the following plots we used the dimensions of one of our coils: $L = 18\,\mathrm{mm}$, $r_i = 11.5\,\mathrm{mm}$ and the PCB thickness of $b = 1.6\,\mathrm{mm}$. When plotting the err_{rel} as a function of β, the maximum relative error is reached when $\beta = 0$ or $\beta = \pi/N$ as illustrated in Fig. 10 and Fig. 11, top drawing. In the bottom drawing the relative error as function of the number N of used windings and the factor A is shown. The conclusions are the same as for the Hall sensor case and also here the error can be limited when using a case. In the prototype A is below 0.5 for I_r and A is above 3 for I_r. In general, as soon as a coil has more than 20 windings, the relative error is below 1%.

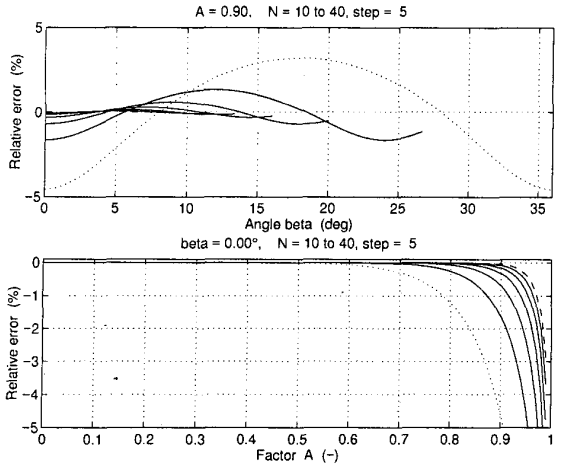

Fig. 10. Coil sensor: relative error of an off-center wire

D. Error prediction

The worst case full scale error in percent or the class index of this probe Fig. 3 for a ramp current signal is given by (31) where d represents the damping ratio $d = T_1/(2T_2)$, $g = di/dt$ is the ramp steepness, f_n is the undamped natural frequency of the coil and I_{FS} is the full scale current of the probe [13].

$$class\ index = 100\,\frac{g}{2\,\pi\,f_n\,I_{FS}}(0.66d^3 - 0.18d^2 + 0.53d + 1) \tag{31}$$

For a symmetrical trapezoidal current signal, having a maximum current value of +/- I_{max} and a steepness of its edges (rising and falling) of g, the worst case error is less than twice the value of (31). With $d = 0.2$ the worst case class index of the probe for the trapezoidal waveform, for all frequencies,

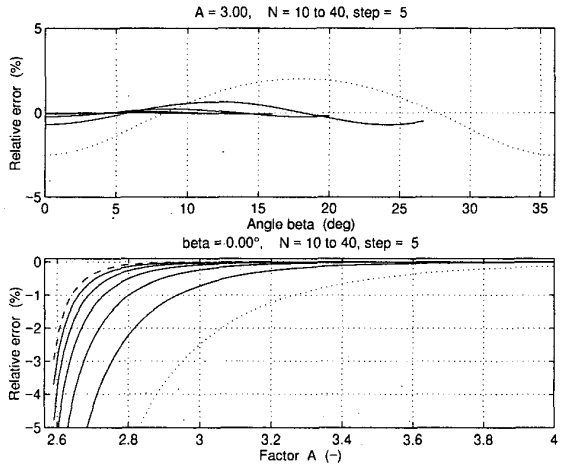

Fig. 11. Coil sensor: relative error of the return wire

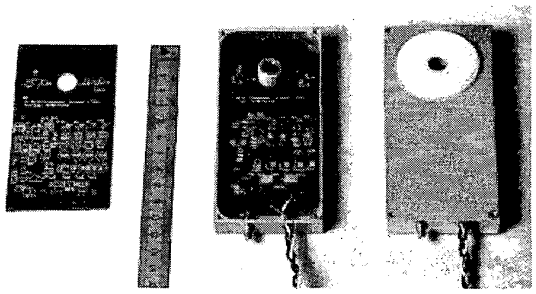

Fig. 12. Probe prototype

with $I_{FS} = I_{max}$ can be expressed by:

$$class\ index = 110\,\frac{g}{\pi\,f_n\,I_{FS}}. \tag{32}$$

The damping ratio d should be kept small and its value is mostly below 0.2.

IV. Measurements

To be able to verify this new principle a prototype as well as a measurement setup to generate high di/dt's was built. With this setup we were able to perform several measurements to compare the HOKA probe with those comercially available.

A. Probe prototype

The probe prototype has been realized on a multi-layer PCB as displayed in Fig. 12. On the left and right side of the hole in the PCB, where the current bar passes through, the two Hall sensors are placed. The coil is implemented on the multi-layer PCB around the hole. Both sensors as well as all electronic components are placed in the case.

B. Measurement setup

B.1 Operating principle

In order to test the accuracy of different current measurement sensors, a setup was needed which can generate the required di/dt of several $\mathsf{kA}/\mu\mathsf{s}$. Errors due to the proximity of current conducting elements can be analyzed as well as the noise immunity to high di/dt. External fields which may lead to errors must be easy to generate. We choose a buck converter topology as shown in Fig. 13. A capacitor battery C is charged by a variable DC-power source. The *IGBT*-switch S is turned on according to the pattern shown in Fig. 14a). The current rise can be described with

$$i_L = \frac{V_C - v_{AK}}{R}\left(1 - e^{-t\frac{R}{L}}\right). \tag{33}$$

Since the sum of the stray inductances in the loop A, represented by $L_\sigma < 1\,\mu\mathsf{H}$, is much smaller than $L = 80\,\mathsf{mH}$, L_σ can be neglected. A voltage drop of V_c of 20% is tolerated during the first phase. The time interval $t_2 - t_1$ is used to define the maximum current I_0 which is measured. At t_2 the currents i_K

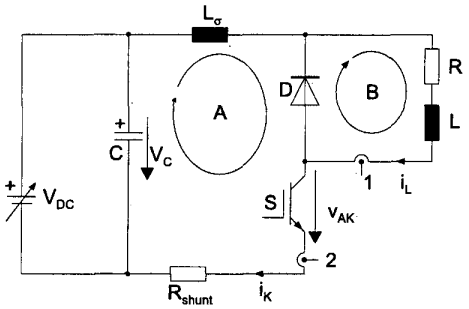

Fig. 13. Test setup configuration

and i_L are equal and the IGBT S is turned off. The current commutates to the freewheeling diode D. The commutation speed di_K/dt is mainly defined by the properties of S as well as L_σ. At t_3 S is turned on and the current i_L flows again through it. The overshoot of i_K is due to the reverse recovery current of D. From t_4 the current i_L is flowing through the loop B. The current decrease is given by

$$i_L(t) = i_L(t = t_4)e^{-t\frac{R}{L}}. \tag{34}$$

With the realized current measurement setup current sensors can be tested for their behavior when measuring slow current transients as well as fast current transients. Fast current transients are only achievable if L_σ is low (typical below 500 nH) and the IGBT driving circuit is very fast.

B.2 Realization

In order to reduce L_σ, strip conductors (Fig. 15) have been used to interconnect the capacitors with the power semiconductors. The IGBT switch and the diode are located in a single power module. The gate drive is mounted straight on top of the module (Fig. 16). So it is possible to reduce the stray inductance in the gate-drive path and the switching speed of the IGBT can be increased. A control loop as proposed in [14] is introduced to reduce the switching speed of the IGBT. Therefore the current transients can be adjusted without inserting extra inductance.

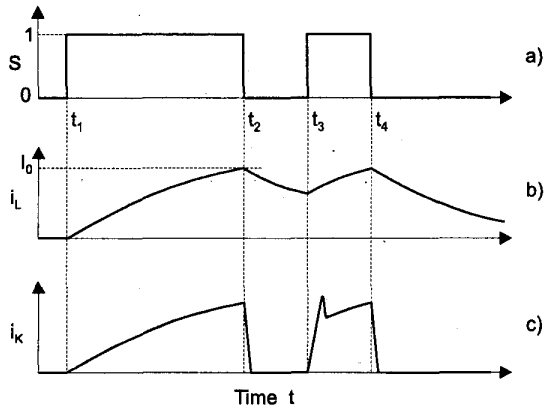

Fig. 14. Curves

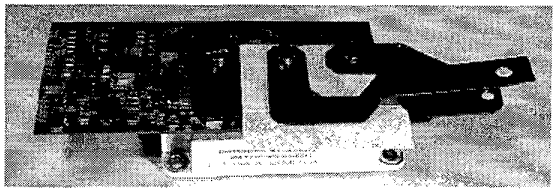

Fig. 15. IGBT with driver PCB and copper strips

A current sensor can be introduced in two different positions namely point 1 or point 2 in Fig. 13. i_L (point 1) is used to measure slow current transients and the influence of external stray fields. Since the extra stray inductance introduced by current probes is not relevant in this point, various current sensors can be inserted and tested. i_K (point 2) is used to measure fast current transients. The HOKA current probe was inserted here to generate the measurement that follows. A coaxial shunt [1] is used as reference.

A control panel allows to adjust the times t_2, t_3 and t_4 individually. The test setup is shown in Fig. 17.

B.3 Measurements

In in the top drawing of Fig. 18 (10 μs/div) the measured curve of a double pulse like in Fig. 14c) is shown. The solid line represents the shunt measurement while the dashed line is the output of the prototype. The bottom drawing shows the relative error when the two signals are treated numerically to form a relative error. The spikes are mainly caused by the data aquisition and they disappear when the time scale is changed. In Fig. 19 (100 ns/div) the trailing edge is displayed. The curve of a second current probe [2] is also shown. Its output signal is represented by the dotted line. Last a rising edge with a di/dt of a little less than 1 kA/μs is shown in Fig. 20 (100 ns/div). Further comparisons for a slow pulse (5 ms) with a 410 Pearson current transformer and an ILA SMZ 200 clamp-on current probe can be found in [15].

[1] LEM 25/10
[2] PEM CWT 15

Fig. 16. IGBT with driver PCB and short gate connection

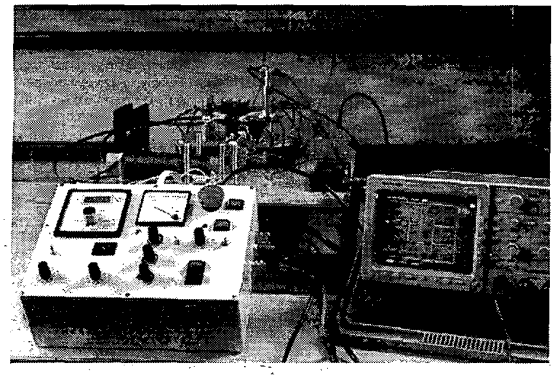

Fig. 17. High power current measurement setup

V. Conclusion

A current probe prototype based on the current measuring principle HOKA has been realized. A description of the evaluation circuit as well as of the geometry of the Hall sensors and air coil is given. The measurement setup to test the prototype is outlined. The measurements carried out with this probe demonstrate the validity of this new principle. Formulas to compute the probe's noise immunity are presented for the case of a filament current wire. The prototype shows a full scale error of +/- 5% for DC as well as for di/dt in the range of some $\mathrm{kA}/\mu\mathrm{s}$. Further research is performed to reduce the overall size of the probe and to increase its accuracy.

References

[1] A. P. Chattock, "On a magnetic potentiometer," *Philosophical Magazine and Journal of Science*, vol. XXIV, no. 5th Series, pp. 94–96, Jul-Dec 1887.

[2] W. Rogowski and W. Steinhaus, "Die Messung der magnetischen Spannung (Messung des Linienintegrals der magnetischen Feldstärke.)," *Archiv für Elektrotechnik*, vol. 1, no. 4, pp. 141–150, 1912.

[3] Klemens Heumann, "Messung und oszillographische Aufzeichnung von hohen Wechsel- und schnell veränderlichen Impulsströmen," *Techn. Mitt. AEG-TELEFUNKEN*, vol. 60, no. 7, pp. 444–448, 1970.

[4] Arthur Radun, "An alternative low-cost current-sensing scheme for high-current power electronics circuits," *IEEE Transactions on Industrial Electronics*, vol. 42, no. 1, pp. 78–84, February 1995.

[5] W. F. Ray and K. D. Murray, "The use of Rogowski coils for current waveform measurement in power electronic circuits," *EPE Power Electronics and Applications*, pp. 3/379–3/383, 1991.

[6] Robert J. Thomas, "High-impulse current and volatge measurement," *IEEE Trans. on Instrumentation and Measurement*, vol. 19, no. 2, pp. 102–117, May 1970.

[7] D. G. Pellinen, "A subnanosecond risetime fluxmeter," *The review of scientific instruments*, vol. 42, no. 5, pp. 667–670, May 1971.

[8] D. G. Pellinen and P. W. Spence, "A nanosecond risetime magampere current monitor," *The review of scientific instruments*, vol. 42, no. 11, pp. 1699–1701, November 1971.

[9] P. Hofer-Noser and N. Karrer, "Monitoring of paralleled IGBT/diode modules," *IEEE Trans. on Power Electronics*, May 1999, in press.

[10] *Tektronix: Instructions A6303 Current Probe*, 1981.

[11] U. Tieze and Ch. Schenk, *Halbleiter-Schaltungstechnik*, Springer, Berlin, 9 edition, 1989.

[12] Jim Williams, *High Speed Amplifier Techniques*, Linear Technology, Milpitas, CA, application note 47 edition, 1991.

[13] N. Karrer, P. Hofer-Noser, and Daniel Henrard, "A new current probe with a wide bandwidth," *Conference EPE'99*, September 1999, in press.

[14] Ch. Gerster and P. Hofer, "Gate-controlled dv/dt and di/dt-limitation in high power igbt converters," *EPE*, vol. 5, no. 3/4, pp. 11–16, January 1996.

[15] N. Karrer and P. Hofer-Noser, "A new current measuring principle for power electronic applications," *Proc. ISPSD'99*, pp. 279–282, May 1999.

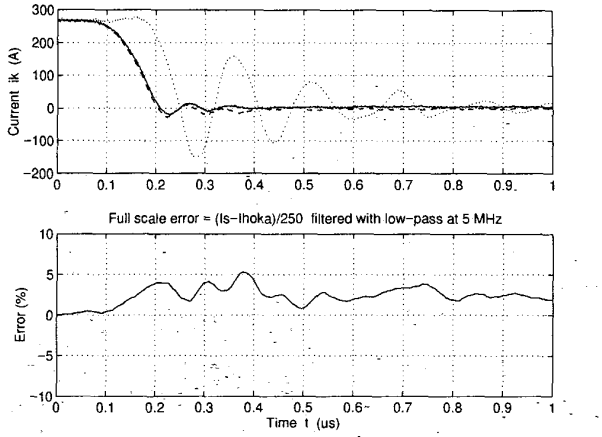

Fig. 19. Trailing edge, $di/dt = 3.0\,\mathrm{kA}/\mu\mathrm{s}$

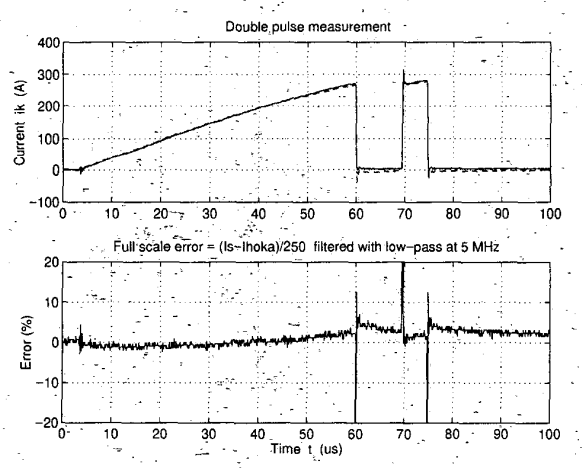

Fig. 18. Double pulse measurement

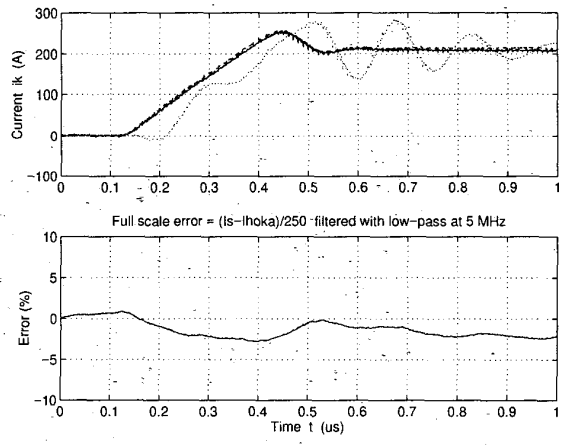

Fig. 20. Rising edge with reverse recovery of diode